An Ultra-Reliable MMW/FSO A-RoF System Based on Coordinated Mapping and Combining Technique for 5G and Beyond Mobile Fronthaul

Rui Zhang, Feng Lu, Mu Xu, Siming Liu, Peng-Chun Peng, Shuyi Shen, Jiale He, Hyung Joon Cho, Qi Zhou, Shuang Yao, and Gee-Kung Chang, *Fellow, IEEE, Fellow, OSA*

***Abstract*—We propose and experimentally demonstrate, for the first time, a system which integrates millimeter-wave (MMW) and free-space-optics (FSO) analog radio-over-fiber (A-RoF) channels, and provides enhanced reliability in 5G and beyond mobile fronthaul (MFH) links. The integrated system utilizes a novel coordinated mapping and combining (CMC) technique that senses the signal quality in each data block and apportions the load accordingly. Furthermore, the technique takes advantage of the abundant bandwidth in both MMW and FSO links and is compatible with orthogonal frequency division multiplexing (OFDM). In the CMC design, the data blocks at the transmitter side are interleaved and repeated in both the frequency domain and the time domain, and then the duplicated blocks are combined with adaptive weight coefficients at the receiver side. We demonstrate experimentally that the proposed CMC technique improves power margins and enhances the robustness of the adaptive diversity combining technique (ADCT)-based FSO/MMW links by mitigating system impairments caused by frequency/time burst interference and power fading attributable to adverse weather conditions. In experiments, compared with the ADCT-based system, we find a 9dB gain in received optical power (ROP) tolerance and a 5.8dB lower EVM floor under a deliberately injected 20-MHz LTE frequency interference burst.**

***Index Terms*— Mobile fronthaul, Radio over fiber technology, Optical fiber communication, Millimeter-wave communication, Free space optical communication.**

I. Introduction

As the fifth generation (5G) mobile technology standards approach finalization in 2019 ahead of product deployment expected by 2021, the 5G ultra-dense, small cell network with simplified remote radio units (RRUs) has emerged as one of the critical enablers of high data rate, high spectral efficiency, and adaptive mobile fronthaul (MFH) networks [1, 2]. Additionally, the cloud radio access network (C-RAN) framework with a high-degree centralization of baseband units (BBUs) is a promising candidate for the massive densification of in-building or outdoor small cells [3, 4]. On the other hand, new services, such as the mission-critical Internet of Things (IoT), require ultra-low latency, extremely high reliability and availability [5, 6]. Therefore, mobile fronthaul links, which connect BBU to remote radio units (RRUs), face a myriad of challenges, among which are: reliability, efficient centralization, cost-efficiency, scalability, low latency and flexibility [5-7]. A two-level, Next Generation Fronthaul Interface (NGFI) has been proposed as a standard to fulfill the needs of C-RAN. It divides traditional BBU into two logical entities: a central unit (CU) and distributed unit (DU), supporting one-to-many flexible connections between a CU and plural DUs, as a strategy to facilitate the functions of joint multi-cell signal processing, coordinated Multi-point (CoMP) transmission and increased resource utilization across multiple cells [6-10]. In the case of fronthaul links between DU and RRUs, it is generally known that analog radio-over-fiber (A-RoF) stands out as having higher bandwidth efficiency, lower cost and smaller latency than digital C-RAN [9-11]. However, deployment of a fiber infrastructure is generally expensive in densely-populated urban areas and may require subsidies in areas where fibers are unavailable, to wit, suburban and rural areas [12, 13]. In view of their easy deployment and ample frequency bandwidth and directionality, millimeter wave (MMW) and free space optics (FSO) has been demonstrated to provide service in the absence of or in addition to fiber links [12-18].

In cases where high reliability and low latency are important, a resilient MFH which incorporates an all-spectrum strategy comprising A-RoF, MMW and FSO may be considered. Optical fibers are subject to mechanical damage, while MMW and FSO are sensitive to weather conditions, and channel interferences. FSO is sensitive to fog, haze while MMW suffers from interference from other MMW channels, rain, frequency selective channel and time-variant channel, which will induce frequency/time burst distortion and power attenuation [19-23]. The aforementioned all-spectrum reliability strategy may be implemented by adaptively combining the two complementary links, MMW and FSO, in order to enhance the reliability of the

R. Zhang, F. Lu, M. Xu, S. Liu, S. Shen, J. He, H. Cho, Q. Zhou, S. Shuang D. Guidotti and G.-K. Chang are with the School of Electrical and Computer Engineering, Georgia Institute of Technology, Atlanta, GA 30308 USA (e-mail: ruizhangece@gatech.edu; fenglu@gatech.edu; xumu@gatech.edu; ssyzoe@gatech.edu; siming.liu@ece.gatech.edu; jiale.he@ece.gatech.edu; hyungjch@gatech.edu; qi.zhou@gatech.edu; shuangyao68@gatech.edu; gkchang@ece.gatech.edu).

P.-C. Peng is with the Department of Electro-Optical Engineering, National Taipei University of Technology, Taipei 10608, Taiwan. (e-mail: pcpeng@mail.ntut.edu.tw)

hybrid wireless system under different weather conditions, as was previously reported [24-26]. However, the ADCT-based system previously developed fails to address the needed tolerance to power attenuation in FSO link and frequency/time-burst distortion in MMW link. Moreover, the previous integrated MMW/FSO system underutilized the FSO bandwidth in order to fit with the narrower MMW, leading to a significant waste of bandwidth resources.

In this paper, we propose and experimentally demonstrate a coordinated mapping and combining (CMC) technique that enables the implementation of an ultra-reliable, CMC-based, integrated MMW/FSO A-ROF system. As shown in Fig. 1, higher-layer data from CUs is processed in DUs. For the access link with a few kilometers or less where fibers are not available, we employ the proposed cost-effective A-RoF-based MMW/FSO system. In all cases, we use spectrally efficient OFDM QAM signaling. At each RRU shown in Fig. 1, we firstly recover the original QAM symbols from each link independently using the corresponding CMC technique. Then the ADCT algorithm is applied to both MMW and FSO symbols to optimize performance. Finally, the recovered signals are transmitted to users. The CMC technique exploits the abundant FSO and MMW bandwidth and shows superior performance in reliability and sensitivity compared to the ADCT-based system. The CMC-based system can satisfy the 3.5% EVM requirement under frequency-burst interference. Moreover, if the weather conditions are optimal for each wireless link, then each link can transmit different information, which enhances the overall capacity.

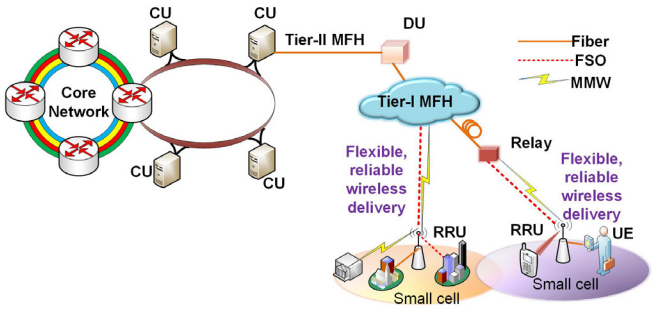

Fig. 1. The architecture of the hybrid FSO/MMW system based network.

This paper is organized as follows. Section II gives a detailed analysis of the working principles of the proposed CMC technique. In Section III, we describe details of the experimental setup. Section IV presents and discusses experimental results, while section V provides concluding remarks.

II. Principles of Operation

The CMC system consists of two parts: coordinated mapping at the transmitter side and coordinated combining at the receiver side. Coordinated combining is the inverse process of coordinated mapping. These two parts optimize the system's reliability and performance.

A. Coordinated mapping at the transmitter side

The CMC mapper is specially designed for OFDM modulation formats widely adopted by 4G, 5G new radio, and Wi-Fi standards. As an example, assume that the number of the original data blocks in the time domain and frequency domain is N_t and N_f, respectively. The time_duration of the original signal is T and frequency spacing of each block is Δf. When the mapping ratio is M, the mapper expands the number of blocks in the time domain to $M \times N_t$ and the frequency spacing of the block to $M \times \Delta f$.

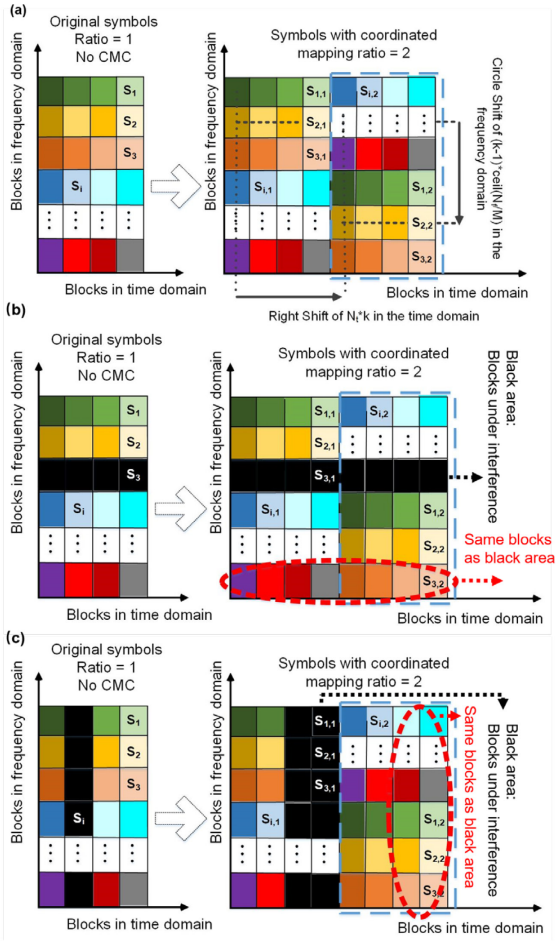

Fig. 2. Working principles of the coordinated mapping (mapping ratio = 2). (a) Scheme of the mapper in coordinated mapping. (b) Mapped signals under frequency-burst interference. (c) Mapped signals under time-burst interference. (Number of distorted blocks increase due to symbol duration shrinking for higher sampling rate.).

The i_{th} block $S_i\left(1 \le i \le N_t \times N_f\right)$ of the original signal is $\Delta f_i = \Delta f$ wide in frequency and $\Delta t_i = \frac{T}{N_t}$ long in time. It is repeated and mapped to M blocks through the following equations:

$$S_{i,k}\left(\Delta t_{i,k}, \Delta f_{i,k}\right) = \mathrm{S}_i\left(\Delta t_i, \Delta f_i\right), \tag{1}$$

$$\Delta t_{i,k} = \frac{\Delta t_i}{M} + \left(k-1\right) \times \frac{T}{M}, \tag{2}$$

$$\Delta f_{i,k} = \left[\left(\Delta f_i - \mathrm{int}\left(\frac{N_f}{M}\right) \times \left(k-1\right) \times \Delta f\right) \mathrm{mod}\left(N_f \times \Delta f\right)\right] \times M, \tag{3}$$

where $S_{i,k}$ is the same as $S_i\,(1 \le k \le M)$ as in Eq. (1). $\Delta t_{i,k}$ and $\Delta f_{i,k}$ are time duration and frequency increment of the k_{th} repeated block, respectively. In Eq. (3), the *int* operator rounds off to the nearest integer and the *mod* operator returns the modulus of a number. The mapping procedure is determined by mapping ratio M and the number of data blocks in the frequency and the time domains.

Fig. 2 (a) shows one example of mapping procedure with mapping ratio M = 2. Same color blocks represent same information content. Eq. (2) shifts or increments the duplicated block in the time domain, while Eq. (3) circle shifts data blocks in the frequency domain. The mapper ensures that the same data blocks are orthogonal in the frequency domain and that the minimum spacing between blocks is maximized by interleaving the duplicated blocks using even interleaving distances. The dispersive distribution makes the signal less susceptible to burst distortions. Fig. 2 (b) and (c) show CMC operation in the presence of frequency-burst interference and time-burst interference. The black area represents the distortion due to interference. Without CMC, data blocks in the frequency domains subject to frequency interference will suffer severe performance degradation. The mapping ensures that there are surviving, unaffected frequency duplicate data blocks that can be recovered, as shown in the circled area in Fig. 2 (b). For example, although $S_{3,1}$ is distorted, $S_{3,2}$ can be used to recover S_3. Then we can use the corresponding coordinated combining techniques to recover the distorted blocks with the duplicated information in other frequency locations, thus showing how ample bandwidth can be the trade-off for increased link reliability. Resiliency to time-burst interference can be treated the same way, as shown in Fig.2 (c). Suppose the original time duration per data block is T/N_t, it is worth noting that due to a higher sampling rate for a higher mapping ratio M, the time duration of every data block reduces to $T/(N_t M)$ as depicted in Fig.3 (a). The number of affected or degraded data blocks increases with the constant duration of the time-burst interference. Thus, in Fig.2 (c), the number of affected data blocks are doubled in the time domain.

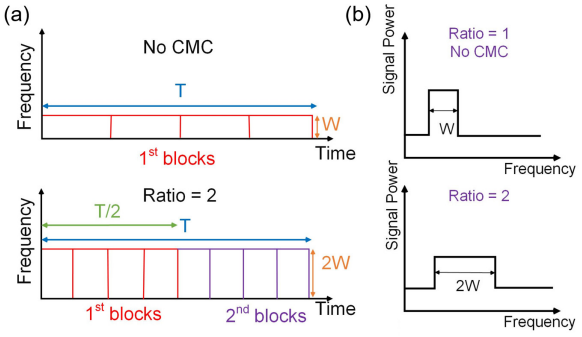

Fig. 3. (a) Schematic representation of the signal in the frequency and time domains. Expanded bandwidth for higher ratios. (M = 1, 2). (b) Frequency spectrum of the mapped signals. Decreased SNR for higher ratios. (M = 1, 2).

Resiliency benefits are obtained at the expense of occupying more bandwidth and lower signal power assigned to each block for a fixed signaling power. As depicted in Fig. 3, as the mapping ratio increases, the required bandwidth increases with increasing sampling rates because the block time duration remains unchanged. Thus, the required bandwidth increases with increasing sampling rate. If the original bandwidth is W, then the bandwidth becomes $M \times W$ for mapping ratio M. The bandwidth cost is not the issue since both MMW link and FSO link have ~~the~~ sufficient bandwidth. Another cost is shown in Fig. 3 (b). With a constant signal power and white background noise, a higher mapping ratio means more data blocks and proportionally lower signal power and lower signal to noise ratio for each block. Thus, in Fig. 3 (b), the amplitude of the spectrum decreases with rising ratios. There is a trade-off between mapping ratio and SNR for fixed signaling power. However, under ordinary circumstances there remains the option of increasing the signal power at the expense of overall power consumption.

B. Coordinated combining at the receiver side

Coordinated combining is the inverse process of coordinated mapping. It adaptively recovers the repeated blocks in both the MMW and FSO links. Given the independent and additive noise and interference in the channel, at the DU, the received i_{th} block signal in the k_{th} slot location is represented by $g_{i,k}$, and consists of the original signal S_i divided by M and an additive noise term, $n_{i,k}$. Here we combine the M copies of the i_{th} blocks dynamically with the coefficients $\gamma_{i,k}\,(1 \le k \le M)$ to get the recovered i_{th} block G_i,

$$G_i = \sum_{k=1}^{M} \gamma_{i,k} g_{i,k} = \sum_{k=1}^{M} \gamma_{i,k} \left(S_i + n_{i,k} \right). \tag{4}$$

The optimal coefficients should minimize the EVM of G_i. Since the EVM estimation is equivalent to $\sqrt{1/SNR}$, we should maximize SNR of G_i, which is SNR_i in [27]. If we set the weight of each repeated block as

$$\gamma_{i,k} = \frac{SNR_{i,k}}{\sum_{k=1}^{M} SNR_{i,k}} = \frac{\dfrac{1}{EVM_{i,k}^2}}{\sum_{k=1}^{M} \dfrac{1}{EVM_{i,k}^2}}. \tag{5}$$

Then, from Eq. (4) and (5), the SNR_i can be written as

$$SNR_i = \frac{\left[\sum_{k=1}^{M} \gamma_{i,k} S_i\right]^2}{\sum_{k=1}^{M} \gamma_{i,k}^2 n_{i,k}^2} = \frac{S_i^2 \left[\sum_{k=1}^{M} \gamma_{i,k}\right]^2}{\sum_{k=1}^{M} \gamma_{i,k}^2 n_{i,k}^2} = \frac{1 \cdot S_i^2}{\sum_{k=1}^{M} \gamma_{i,k}^2 n_{i,k}^2}$$
$$= \frac{1}{\sum_{k=1}^{M} \dfrac{\gamma_{i,k}^2 n_{i,k}^2}{S_i^2}} = \frac{1}{\sum_{k=1}^{M} \dfrac{\gamma_{i,k}^2}{SNR_{i,k}}} = \sum_{k=1}^{M} SNR_{i,k}. \tag{6}$$

The weight $\gamma_{i,k}$ yields the optimal SNR_i since the SNR of the final block never exceeds the sum of the SNR_i of each sub-block according to the maximal ratio combining principle [25]. Based on the analysis above, we propose the following coordinated combining methodology.

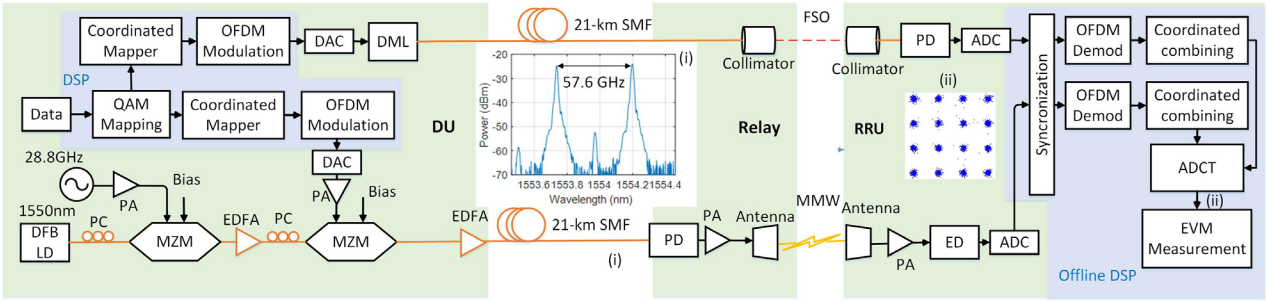

Fig. 4. Experimental setup of the CMC-based hybrid FSO/MMW A-RoF system. (i) Optical spectrum. (ii) Constellation of the recovered baseband QAM signal. PA: power amplifier, DAC: digital-to-analog converter, DML: directly modulated laser, DFB: distributed feedback laser, PC: polarization controller, MZM: Mach Zehnder modulator, EDFA: Erbium-doped fiber amplifier, PD: photodetector, ED: envelope detector, ADC: analog-to-digital converter, ADCT: adaptive diversity combining technique.

Assume the mapping ratios for MMW and FSO are M_1 and M_2, respectively. Both links are combined in the same data blocks using the following equations:

$$S_{MMW,i}\left(\Delta t_i,\Delta f_i\right)=\sum_{k=1}^{M_1}\alpha_{i,k}\left(S_{MMW,i,k}\left(\Delta t_{i,k},\Delta f_{i,k}\right)\right), \tag{7}$$

$$\alpha_{i,k}=\frac{\frac{1}{EVM_{MMW,i,k}^2}}{\sum_{k=1}^{M_1}\frac{1}{EVM_{MMW,i,k}^2}}, \tag{8}$$

$$S_{FSO,i}\left(\Delta t_i,\Delta f_i\right)=\sum_{k=1}^{M_2}\beta_{i,k}\left(S_{FSO,i,k}\left(\Delta t_{i,k},\Delta f_{i,k}\right)\right), \tag{9}$$

$$\beta_{i,k}=\frac{\frac{1}{EVM_{FSO,i,k}^2}}{\sum_{k=1}^{M_1}\frac{1}{EVM_{FSO,i,k}^2}}. \tag{10}$$

The $\Delta t_{i,k}$ and $\Delta f_{i,k}$ can be obtained from Eqs. (2) and (3), $S_{MMW,i,k}$ and $S_{FSO,i,k}$ are the k_{th} mapped block of the i_{th} original block, $\alpha_{i,k}$ and $\beta_{i,k}$ are the weights for $S_{MMW,i,k}$ and $S_{FSO,i,k}$, respectively. $S_{MMW,i}$ and $S_{FSO,i}$ are the i_{th} recovered blocks from the combining operation. $EVM_{MMW,i,k}$ and $EVM_{FSO,i,k}$ are calculated from blind EVM estimation. Since the weights in Eqs. (8) and (10) are inversely proportional to the calculated EVM, they can optimize the system performance adaptively. After coordinated combining, ADCT is used to combine the MMW symbols and FSO symbols to get the final QAM symbols.

III. Experiment Setup

Fig. 4 depicts the experimental setup of the CMC-based hybrid FSO/MMW A-RoF system. The testbed consists of one DU, one Relay and one RRU. Given a bandwidth of 576 MHz and a mapping ratio *M*, the transmitted 16QAM OFDM signal has a bandwidth of $576\times M$ MHz with $480\times M$ -kHz subcarrier spacing, 3.125% cyclic prefix (CP) and 2-Gbps data rate.

At the DU, after mapping the high-layer data to QAM symbols, the symbols are split into two branches and mapped independently using coordinated mappers with optimized mapping ratios, followed by OFDM modulation. Then the OFDM symbols are fed into a digital-to-analog converter (DAC) for the electrical signal generation. For FSO, we employ the intensity-modulation-direct-detection (IM-DD) scheme by using a directly modulated laser (DML). For MMW, a 1550nm distributed feedback (DFB) laser is used as light source, which is modulated by a Mach–Zehnder modulator (MZM) driven sinusoidally by a 28.8-GHz microwave source to produce a MMW carrier on a subsequent photodiode. A second MZM is used to modulate data onto the MMW carrier. Two polarization controllers (PCs) are used to maintain optimal polarization alignment for modulation.

After transmission via a 21-km single mode fiber (SMF), one branch of the signal is detected by a photo-detector (PD) in the relay node (Fig. 1). An antenna with 25-dBi gain paired with a power amplifier (PA) is used for MMW boosting and transmission. The other branch of the signal is coupled to a collimator for FSO transmission.

At the RRU, a symmetric antenna, followed by a low-noise amplifier (LNA) and envelope detector (ED) are employed to detect and down-convert the MMW signals. A real-time digital sampling oscilloscope (DSO) samples and stores the signals for offline DSP. For the FSO link, a collimator and a PD with 10-GHz bandwidth focus and detect the directly modulated optical signal. In offline-DSP, the sampled data from the MMW and FSO links is first synchronized to remove ~~the~~ path delays. Then the synchronized signals are separately de-mapped using coordinated combining after OFDM demodulation to recover the optimized QAM symbols. Finally, we apply the ADCT algorithm to combine the MMW and FSO signals together in preparation for final EVM measurement and performance analysis.

IV. Experiment Results

As a first step, considering that there is a trade-off between mapping ratios and SNR per data block, we utilize training symbols to find the optimal mapping ratio of MMW link to FSO link. Next, we apply the optimal mapping ratios to both links and evaluate the hybrid system's performance and reliability. It is worth noting that the optimal mapping ratio is fixed for constant output power from the transmitter side in a fixed system.

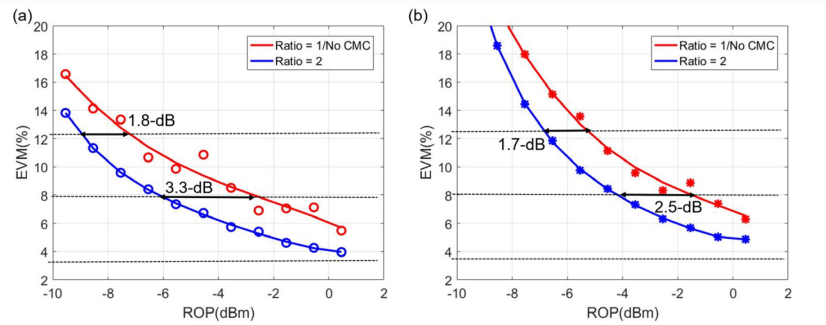

Fig. 5. Experimental results for the MMW link. Power sensitivity performances for the (a) back to back (BTB) experiment and (b) after 21-km SMF.

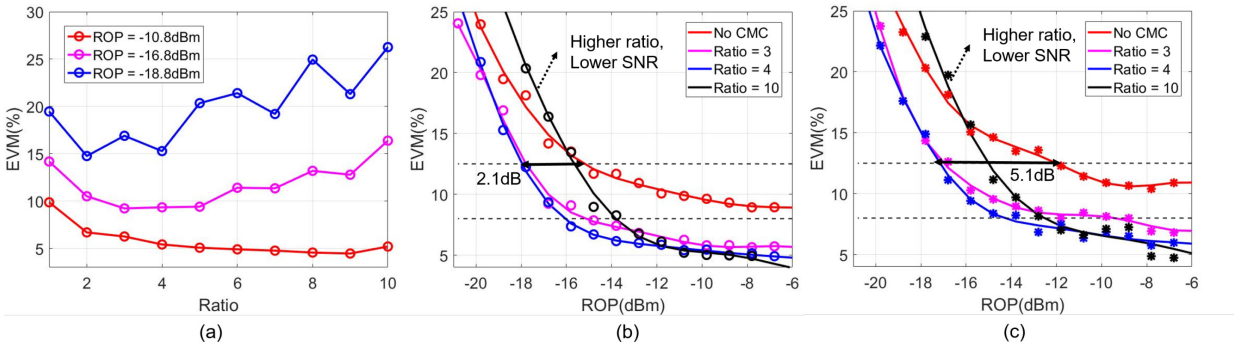

Fig. 6. Experimental results for the FSO link. (a) EVM performance versus mapping ratio for three values of received optical power (ROP). Power sensitivity performance for three mapping rations compared to the case of no CMC (b) BTB measurements and (c) after 21-km SMF.

A. Optimal ratio for MMW

Due to the limited bandwidth of the ED in this experiment, the MMW can only support the mapping ratio M_1 up to two. However, in practice, the bandwidth wouldn't be limited by the ED and the supporting mapping ratio will be larger [28].

Fig. 5 (a) shows the results of power sensitivity measurements in back-to-back (BTB) and after 21-km SMF transmission for two different mapping ratios. Reference lines of 12.5%, 8% and 3.5% EVM are presented. As shown in Fig.5 (a) and (b), the 21-km SMF transmission generates around 2-dB power penalty. Figure 5 (b) shows the MMW signal achieves 1.7-dB/2.5-dB power sensitivity gain with 21-km fiber concerning 12.5%/8% EVM when $M_1 = 2$.

B. Optimal ratio for FSO

The FSO link has a PD-limited bandwidth of 10 GHz and can support a large number of mapping ratios. Fig. 6(a) presents the EVM performance versus mapping ratio from 1 to 10 for three values of received optical power (ROP), -10.8 dBm, -16.8 dBm, and -18.8 dBm. As would be expected, at higher ROP, such as -10.8 dBm, the EVM performance is better, particularly for higher mapping ratios. However, with decreasing ROP, the performance at higher ratios degrades rapidly. The degradation can be attributed to the lower available power, and consequently, the lower S/N ratio per block as the mapping ratio increases as discussed in conjunction with Fig. (3). Therefore, the optimal mapping ratio is limited to between 3 and 4. However, in the system with a dynamic gain to maintain a constant SNR over ROP, the optimal mapping ratio can be extended at the expense of power dissipation. Fig. 6(b) and (c) show the power sensitivity performances with/without mapping at three ratios. EVM reference lines for 12.5% and 8% are shown for reference as in Fig. 5. As in Fig. 5, higher mapping ratios are more sensitive to ROP because of lower SNR per block. By applying the optimal ratio of CMC, the power sensitivity shows 2.1-dB and 5.1-dB improvement in BTB and 21-km SMF transmission experiments. Moreover, the CMC-based signal maintains an 8% EVM floor down to a ROP about -16 dBm while FSO without CMC is not able to achieve 8% EVM. Therefore, by applying CMC, even an FSO link without mapping can still achieve the 8% EVM requirement.

C. Hybrid MMW/FSO A-RoF system performance

Using the optimal mapping ratio obtained from a training sequence, we can measure the performance of the hybrid MMW/FSO A-RoF system. The ratios of MMW and FSO are two and four, respectively.

Fig. 7 shows the experimental results for the combined MMW/FSO system, with 12.5%, 8%, and 3.5% reference lines again included. Fig. 7 (a) shows the minimum ROP required to achieve 8% EVM for both the FSO and MMW links. The single MMW link should satisfy the 8% EVM requirement at –3dBm. The CMC-based hybrid system shows a significant gain compared with the hybrid system without CMC. The ROP tolerance of the MMW link improves 3 dB, 3.6 dB, 4.3 dB and up to 9 dB when the ROP of the FSO link is -21.8 dBm, -19.8 dBm, -17.8 dBm, and -15.8 dBm. In the case of a good FSO channel condition, the ROP tolerance of MMW is very high. Fig. 7 (b) shows the power sensitivity performance for a single MMW link and hybrid MMW/FSO without and with CMC. In the absence of CMC, the hybrid system is able to maintain the EVM level below 8%, but cannot achieve 3.5% EVM with reasonable ROP values. The CMC-based hybrid system can achieve 3.5% EVM when the ROP of the MMW link is higher than -4 dBm. Its EVM floor can reach 4.2% with an improvement of up to 5.8-dB compared to the hybrid system without CMC.

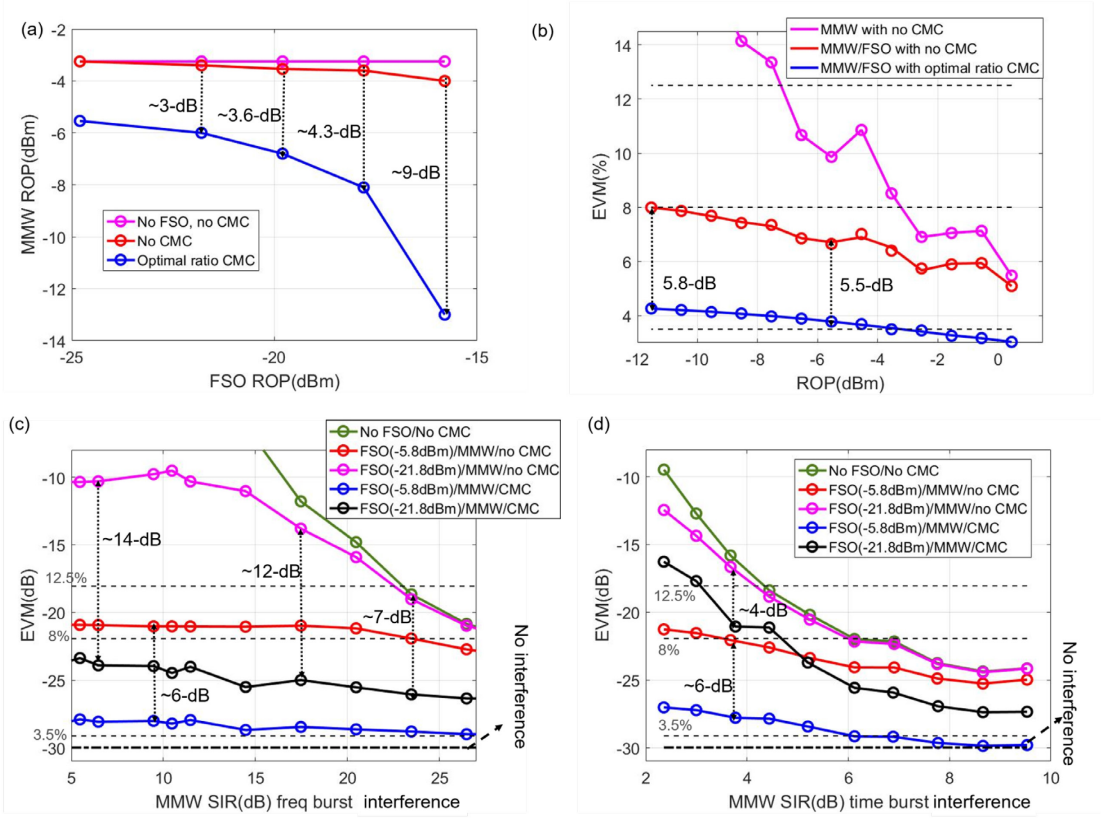

Fig. 7. Experimental results for hybrid MMW/FSO A-ROF system. (a) Benchmarks of ROP required to achieve 8% EVM. (b) hybrid system EVM performance with and without CMC and optimized mapping ratio. (c) EVM performance with 20-MHz frequency-burst interference. (d) EVM performance with time-burst interference.

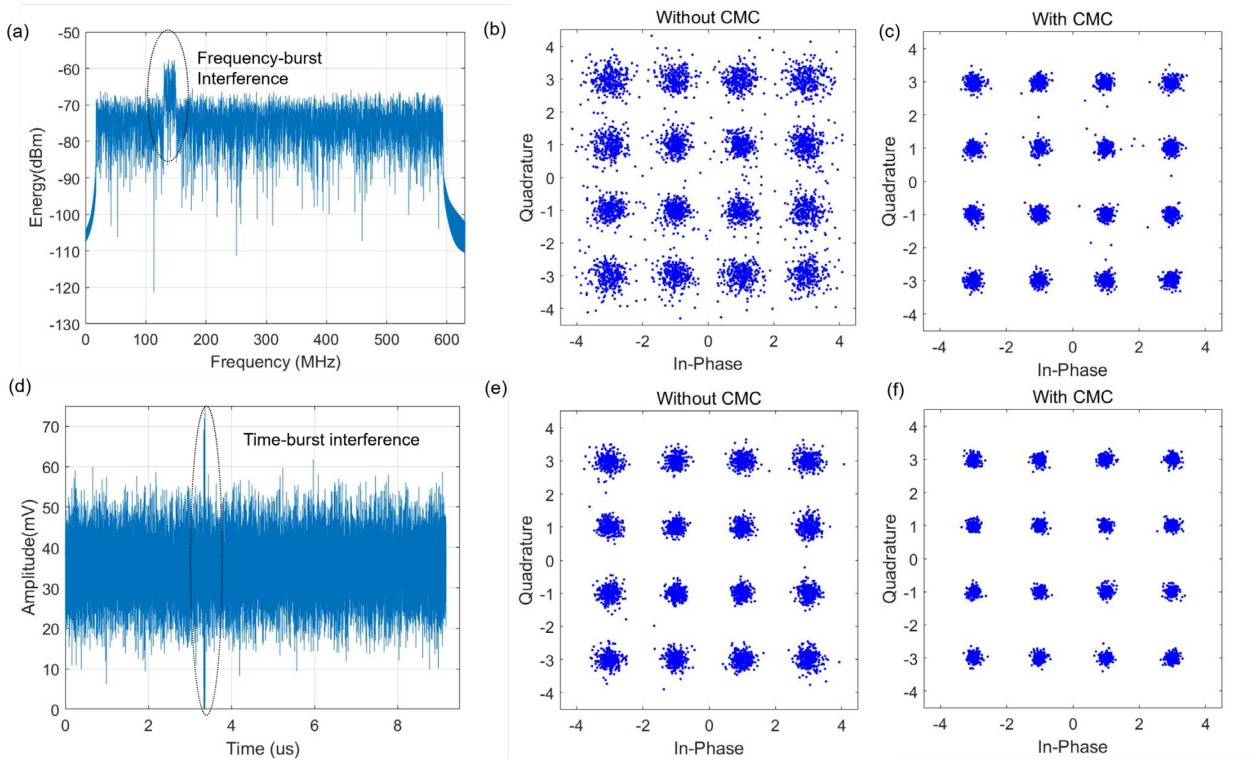

Fig. 8. Transmitted OFDM signal and recovered QAM signal with frequency/burst interference. (a) MMW signal under frequency-burst interference. Constellation of the recovered baseband QAM signal with the frequency-burst interference (SIR = 17dB, ROP of FSO = -21.8 dBm, ROP of MMW = -2 dBm) for the ADCT-based system (b) without CMC (c) with CMC. (d) MMW signal under time-burst interference. Constellation of the recovered baseband QAM signal with the time-burst interference (SIR = 8.7 dB, ROP of FSO = -5.8dBm, ROP of MMW = -2 dBm) for the ADCT based system (e) without CMC (f) with CMC.

There are mainly two types of interferences in the system. 1) A MMW link within an unlicensed frequency band, may suffer from out-of-band interference from an adjacent MMW channel leading to frequency burst interference or time burst interference. 2) The FSO channel is robust against in-band stray light interference in part due to the narrowness of its beam and in part owing to narrow band-pass optical filtering but is susceptible to weather conditions such as atmosphere turbulence, scattering and shading or path blockage, which cause power attenuation or fluctuations. To evaluate the robustness of the hybrid system, we assume an undisturbed ROP and add a simulated wireless interference. Here we simulate two cases of MMW link interference. One is a frequency interference from a MMW channel that transmits a 20-MHz LTE signal and the other is a time burst interference that lasts for around 1/6 of the single-symbol duration. For FSO, we can adjust the attenuator to achieve power attenuation, which is equivalent to the complicated weather or atmospheric interference.

Fig.7 (c) shows the EVM performance versus signal-to-interference ratio (SIR) of the system when MMW is subjected to frequency burst interference. If the FSO is in good channel condition, the CMC shows about 6-dB EVM gain compared to the absence of CMC. The CMC-based system shows less than 2-dB EVM penalty from the no interference dashed reference line. Moreover, the EVM floor is maintained at around 4.2%. The worst case occurs when the MMW is under frequency burst attack and the ROP in the FSO channel is minimal. (e.g., ROP = -21.8 dBm). In this case, the performance of the hybrid system without CMC is severely degraded while that of the CMC-based system maintains EVM below the 8 % reference line. The CMC-based system generates around a 2-dB penalty compared to the no interference reference line. It achieves 6-dB to 14-dB EVM gain compared to its counterpart without CMC.

As illustrated in Fig. 8 (b), the constellation of the recovered QAM signal will be distorted. By utilizing CMC, a good constellation is recovered.

Fig.7 (d) illustrates the EVM performance with SIR variations when the MMW channel is affected by time-burst interference. As shown in Fig.8 (d), the interference lasts for 1/6 of a symbol duration. Similar to Fig.7 (c), the CMC-based hybrid system shows up to 6-dB EVM gain and generates less than the 3-dB penalty when FSO is in good channel condition. It can tolerate 6-dB SIR while keeping the EVM floor as 3.5%. In the worst case, the CMC-based system achieves around 4-dB EVM gain compared with the non-CMC supported system, which almost follows the curve of the single MMW link. Fig.8 (e) and (f) show the constellations of the affected signals after recovery with and without CMC. Without CMC, time-burst interference leads to a worse constellation. With CMC technique, the constellation is better.

V. Conclusion

We have proposed a novel CMC technique for OFDM fiber-wireless signal transport and experimentally demonstrated improved free-space signaling reliability with the use of a CMC-based hybrid MMW/FSO A-RoF system. The CMC system exploits the abundant bandwidth of the transmitted OFDM signals and maps each data block to several separated frequency and time locations using a coordinated mapper. A blind-EVM-estimation-based coordinated combining technique combines every duplicated data block with an optimized weight in both FSO and MMW links independently. Following CMC optimization with the ATDC algorithm yields the optimized signals. In the experiment, the CMC-based system shows enhanced power sensitivity and enhanced robustness to frequency/time-burst interference thanks to the dispersive distribution of the repeated data blocks. We show a 9dB ROP tolerance gain at 8% EVM for the hybrid MMW/FSO system. When the CMC-based hybrid system is operated in fair channel condition, it can satisfy the 3.5% EVM requirement while the non-CMC supported system is unable to achieve this minimal requirement.

Even in extreme operating condition when the MMW signal is under frequency-burst interference and the FSO channel is severely attenuated, the EVM performance of the CMC-based system only exhibits 1-dB to 2-dB penalty while the system without CMC does not work at all. Thus, the proposed CMC-based A-RoF system achieves a milestone accomplishment for an ultra-reliable and more secure 5G and beyond MFH with enhanced system power margins.

References

[1] V. Jungnickel, K. Manolakis, W. Zirwas, B. Panzner, V. Braun, M. Lossow*, et al.*, "The role of small cells, coordinated multipoint, and massive MIMO in 5G," *IEEE Communications Magazine,* vol. 52, pp. 44-51, 2014.

[2] I. Hwang, B. Song, and S. S. Soliman, "A holistic view on hyper-dense heterogeneous and small cell networks," *IEEE Communications Magazine,* vol. 51, pp. 20-27, 2013.

[3] K. Sundaresan, M. Y. Arslan, S. Singh, S. Rangarajan, and S. V. Krishnamurthy, "FluidNet: A flexible cloud-based radio access network for small cells," *IEEE/ACM Transactions on Networking,* vol. 24, pp. 915-928, 2016.

[4] E. Hossain and M. Hasan, "5G cellular: key enabling technologies and research challenges," *IEEE Instrumentation & Measurement Magazine,* vol. 18, pp. 11-21, 2015.

[5] S. Li, L. Da Xu, and S. Zhao, "5G internet of things: A survey," *Journal of Industrial Information Integration,* 2018.

[6] J. Bartelt, N. Vucic, D. Camps-Mur, E. Garcia-Villegas, I. Demirkol, A. Fehske*, et al.*, "5G transport network requirements for the next generation fronthaul interface," *EURASIP Journal on Wireless Communications and Networking,* vol. 2017, p. 89, 2017.

[7] I. Chih-Lin, J. Huang, Y. Yuan, and S. Ma, "5G RAN Architecture: C-RAN with NGFI," in *5G Mobile Communications*, ed: Springer, 2017, pp. 431-455.

[8] I. Chih-Lin, H. Li, J. Korhonen, J. Huang, and L. Han, "RAN Revolution with NGFI (xHaul) for 5G," *Journal of Lightwave Technology,* 2017.

[9] P. Chanclou, L. A. Neto, K. Grzybowski, Z. Tayq, F. Saliou, and N. Genay, "Mobile fronthaul architecture and technologies: A RAN equipment assessment," *Journal of Optical Communications and Networking,* vol. 10, pp. A1-A7, 2018.

[10] Y. M. Alfadhli, M. Xu, S. Liu, P.-C. Peng, and G.-K. Chang, "Real-Time Demonstration of Adaptive Functional Split in 5G Flexible Mobile Fronthaul Networks," in *Optical Fiber Communication Conference*, San Diego, California, 2018, p. Th2A.48.

[11] X. Li, X. Xiao, Y. Xu, K. Wang, L. Zhao, J. Xiao*, et al.*, "Real-time demonstration of over 20Gbps V-and W-band wireless transmission capacity in one OFDM-RoF system," in *Optical Fiber Communications Conference and Exhibition (OFC), 2017*, 2017, pp. 1-3.

[12] C. Liu, J. Wang, L. Cheng, M. Zhu, and G.-K. Chang, "Key microwave-photonics technologies for next-generation cloud-based

radio access networks," *Journal of Lightwave Technology,* vol. 32, pp. 3452-3460, 2014.

[13] A. T. Pham, P. V. Trinh, V. V. Mai, N. T. Dang, and C.-T. Truong, "Hybrid free-space optics/millimeter-wave architecture for 5G cellular backhaul networks," in *Opto-Electronics and Communications Conference (OECC), 2015*, 2015, pp. 1-3.

[14] P. T. Dat, A. Kanno, K. Inagaki, and T. Kawanishi, "High-capacity wireless backhaul network using seamless convergence of radio-over-fiber and 90-GHz millimeter-wave," *Journal of Lightwave Technology,* vol. 32, pp. 3910-3923, 2014.

[15] C. Dehos, J. L. González, A. De Domenico, D. Ktenas, and L. Dussopt, "Millimeter-wave access and backhauling: the solution to the exponential data traffic increase in 5G mobile communications systems?," *IEEE Communications Magazine,* vol. 52, pp. 88-95, 2014.

[16] H.-C. Chien, C. Liu, J. Liu, S.-H. Fan, Y.-T. Hsueh, Z. Jia*, et al.*, "Emerging technologies for mm-wave RoF communication," in *Photonics Society Summer Topical Meeting Series, 2012 IEEE*, 2012, pp. 88-89.

[17] X. Han, L. Chen, X. Li, J. Xiao, and J. Yu, "Optical‐wireless integration of W‐band wireless and free‐space optical links," *Microwave and Optical Technology Letters,* vol. 59, pp. 561-563, 2017.

[18] R. Puerta, J. Yu, X. Li, Y. Xu, J. J. V. Olmos, and I. T. Monroy, "Single-Carrier Dual-Polarization 328-Gb/s Wireless Transmission in a D-Band Millimeter Wave 2× 2 MU-MIMO Radio-Over-Fiber System," *Journal of Lightwave Technology,* vol. 36, pp. 587-593, 2018.

[19] M. El Khaled, P. Fortier, M. L. Ammari, and S. A. M. Tariq, "Optimal power allocation for underground selective channel at 60 GHz," in *Communications Workshops (ICC), 2014 IEEE International Conference on*, 2014, pp. 736-741.

[20] Y. Shoji, C.-S. Choi, and H. Ogawa, "70-GHz-band OFDM transceivers based on self-heterodyne scheme for millimeter-wave wireless personal area network," *IEEE transactions on microwave theory and techniques,* vol. 54, pp. 3664-3674, 2006.

[21] S. Rangan, T. S. Rappaport, and E. Erkip, "Millimeter-wave cellular wireless networks: Potentials and challenges," *Proceedings of the IEEE,* vol. 102, pp. 366-385, 2014.

[22] C.-S. Choi, Y. Shoji, and H. Ogawa, "Implementation of an OFDM baseband with adaptive modulations to grouped subcarriers for millimeter-wave wireless indoor networks," *IEEE Transactions on Consumer Electronics,* vol. 57, 2011.

[23] H. Dahrouj, A. Douik, F. Rayal, T. Y. Al-Naffouri, and M.-S. Alouini, "Cost-effective hybrid RF/FSO backhaul solution for next generation wireless systems," *IEEE Wireless Communications,* vol. 22, pp. 98-104, 2015.

[24] J. Zhang, J. Wang, Y. Xu, M. Xu, F. Lu, L. Cheng*, et al.*, "Fiber–wireless integrated mobile backhaul network based on a hybrid millimeter-wave and free-space-optics architecture with an adaptive diversity combining technique," *Optics letters,* vol. 41, pp. 1909-1912, 2016.

[25] D. G. Brennan, "Linear diversity combining techniques," *Proceedings of the IRE,* vol. 47, pp. 1075-1102, 1959.

[26] F. Lu, M. Xu, S. Shen, Y. M. Alfadhli, H. J. Cho, and G.-K. Chang, "Demonstration of Inter-Dimensional Adaptive Diversity Combining and Repetition Coding in Converged MMW/FSO Links for 5G and beyond Mobile Fronthaul," in *Optical Fiber Communication Conference*, San Diego, California, 2018, p. M3K.4.

[27] H. A. Mahmoud and H. Arslan, "Error vector magnitude to SNR conversion for nondata-aided receivers," *IEEE Transactions on Wireless Communications,* vol. 8, 2009.

[28] C.-H. Ho, W.-J. Jiang, R. Sambaraju, W.-Y. Lee, T.-H. Lu, C.-Y. Wang*, et al.*, "Performance evaluation of a 60 GHz radio-over-fiber system employing MIMO and OFDM modulation," *IEEE Journal on Selected Areas in Communications,* vol. 31, pp. 780-787, 2013.